Robot Design and Experimentation
Final Report

Benjamin Bokser, Nikolai Flowers, Nicholas Jones, Joseph Wood

May 18th, 2021

Abstract

Energy efficiency is an ongoing challenge in the field of legged robotics due to the high energy consumption involved in dynamic locomotion activities. Inspiration can be taken from animals such as kangaroos, which use long tendons to reduce the metabolic cost of jumping. We predict that as tendon extension increases for a given spring constant, the energetic cost of successive hopping to a constant height decreases for a legged robot. A 1-D constrained vertically hopping monopod robot was designed and built with a modular tendon mechanism which allows for discrete adjustments of tendon length. The robot consecutively jumps to a specified height using an adaptive switching controller. The average power consumed at steady state for a specific height is logged for each tendon configuration, showing that as tendon strain increases from 30% to 80%, average power consumed decreases by approximately 20%.

1 Introduction

For many applications, mobile robots must be able to work for long periods of time without recharging in order to be truly viable. However, modern robots are severely limited in this regard by the current state of battery technology. Legged robots in particular are often designed to prioritize simplicity of control rather than energy efficiency, which contributes to their short duty cycles. Boston Dynamics' Spot Mini, a quadruped robot, has a battery life of just 90 minutes despite its $75,000 price tag [1].

Hopping robots possess a series of advantages over other types of legged robots, namely their ability to precisely hit desired footholds in rough terrain [2] and achieve high efficiency from storing energy through contact [3]. In the animal kingdom, large fauna such as gazelles and kangaroos (Figure 1) take advantage of long tendons in their legs which act as springs to store and release energy on each loading cycle [4]. This greatly improves their metabolic efficiency [5].

The use of tendons to introduce spring mechanics in legged robots has been explored widely. Most notably, the 3D Bow Leg Hopper returned about 70% of its mechanical energy on each hop [6]. More recently, Salto, Salto 1-P [3], and Ascento [7] all used series elastic actuators for energy storage. However, the problem of control has usually taken the foreground [8]. In this research, we plan to observe the relationship between tendon length and energy efficiency for a consecutively hopping monopod. The one-dimensional task of hopping is chosen as a starting point in our research of efficient locomotion. As explained in the future work section, our

robotic platform is easily extendable to two-dimensional and eventually unconstrained three-dimensional running and hopping by adding lateral control.

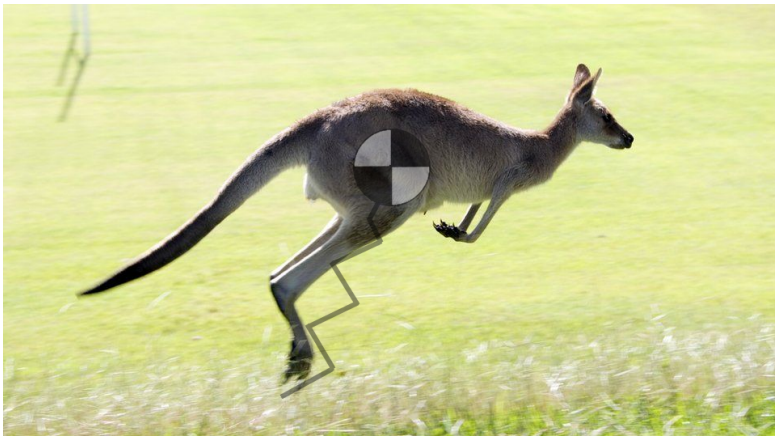

Figure 1: Red kangaroo with SLIP (Spring Loaded Inverted Pendulum) model overlayed. Red Kangaroos have an unusually high efficiency, attributed to elastic energy storage and recovery in their long tendons [5], making them an interesting animal to study for biomechanists and roboticists creating energy-efficient locomotors. (Modified from source: BBC News [9])

2 Hypothesis

As tendon extension increases for a given spring constant, the energetic cost of successive hopping to a constant height decreases for a legged robot.

3 Design

3.1 Mechanical Design

The robot is a lightweight, direct-drive monopod hopper constrained to movement in the vertical axis. Direct drive actuation was chosen for maximal actuator transparency (which improves measurement of torque from motor current and reduces reflected inertia) [10]. In addition, the lack of any gearing reduces the weight of the robot significantly. Permanent magnet synchronous outrunner motors with large air gap radii for their volume were chosen for maximal torque density.

As shown in Figure 2, the motors are connected in series. The use of serial actuation rather than parallel actuation allows us to avoid mechanical antagonism, which would reduce efficiency and interfere with efforts to measure energy loss from other sources [11].

Despite being constrained to vertical movement, the robot has two degrees of freedom (DoF). This allows the design to have the potential to transition to 2D (planar) movement in future work. In addition, the use of just one motor would require a more complex straight-line extensor mechanism. [12].

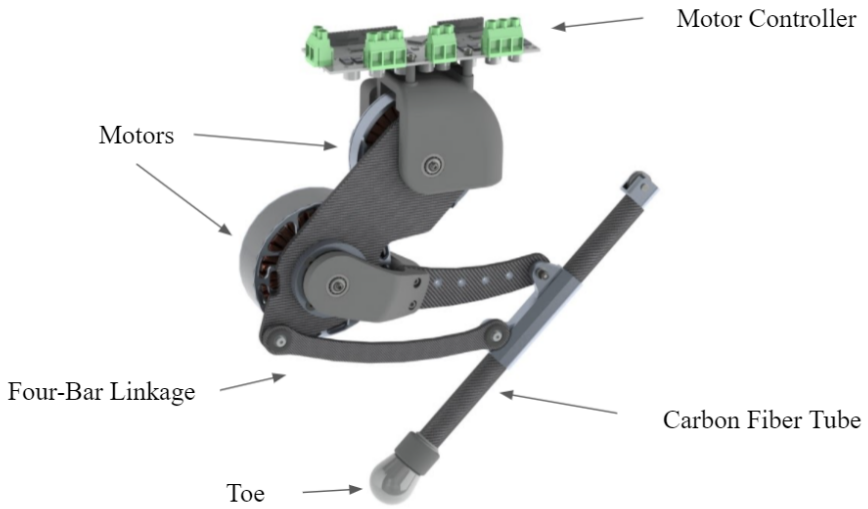

Figure 2: The final design.

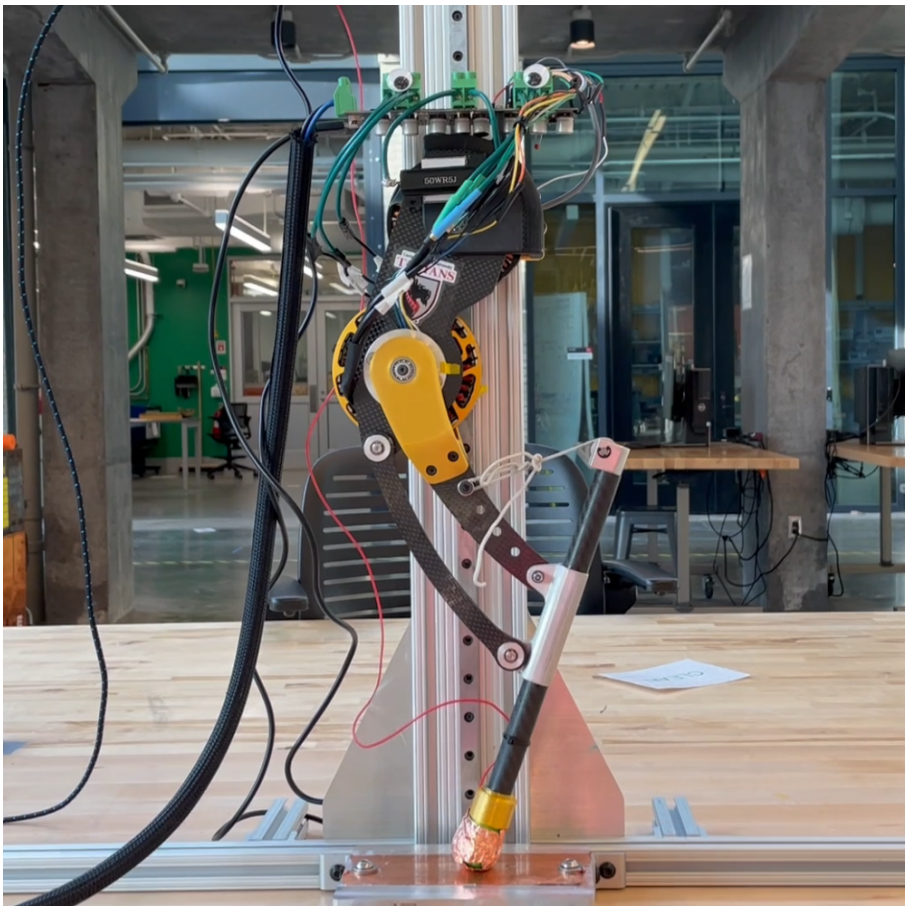

Figure 3: RoboJoey on the test rail.

The first motor rotates the leg about the base of the robot, and the second motor drives extension of the leg through a four-bar parallel mechanism. To properly scale the links, we

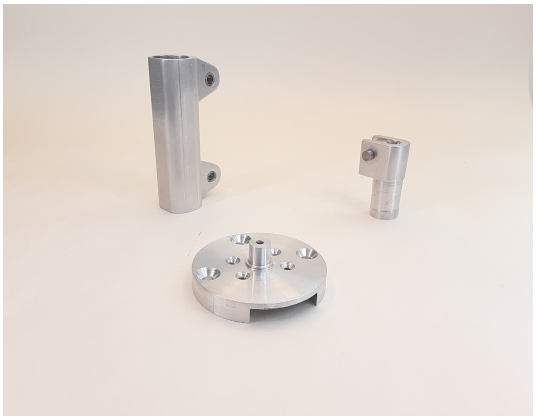

(a) Aluminum components.

(b) CFRP components.

Figure 4: Components fabricated from carbon fiber reinforced polymer (CFRP) and aluminum, which enabled a lightweight leg design.

built a first-order model of the robot hopping in Simulink [13] that executes very quickly in order to perform a search over the design space (of linkage lengths and spring properties). The model assumes a point mass at the hip, massless legs, and generates torque requirements for each motor for a given jump height and frequency. This allowed us to see that in our original design, the motors we selected did not have sufficient torque to jump without a spring. To find design parameters that would allow the robot to jump, we searched over a range of link lengths, and selected a set of link length values that put our required motor torque under the peak torque of 4.7 N*m. This simulation also allowed us to select a spring constant that minimized antagonistic torque between the spring and actuator, but still provided appropriate assist. Figure 13 shows the results of that analysis based on a preliminary mockup design. As a result, the size of the leg was reduced to approximately 0.75x its original size to keep within motor torque limits. In addition, the size of the first (hip) motor was reduced, as less torque is required for that joint.

The structural links are composed of carbon fiber reinforced polymer (CFRP) cut with a waterjet machine. Other components are either 3D-printed from PLA plastic or machined from 6061-T6 aluminum (Figure 4). All bearing joints are preloaded with spring washers to reduce backlash. Hard stops prevent the links from driving past predetermined joint limits. The toe is 3D-printed from TPU with low infill density for impact damping.

The design of the tendon mechanism is shown in Figure 5. The tendon is located inside of the last link, which is a hollow CFRP tube. The tendon is anchored at the bottom of the tube and connected to a steel cable, which is routed around a pulley at the top of the tube to one of four mounting points on the leg. The location of the mounting point affects the extension of the spring as a function of leg flexion, as shown in Figure 15. Spring tension prevents the cable from coming loose.

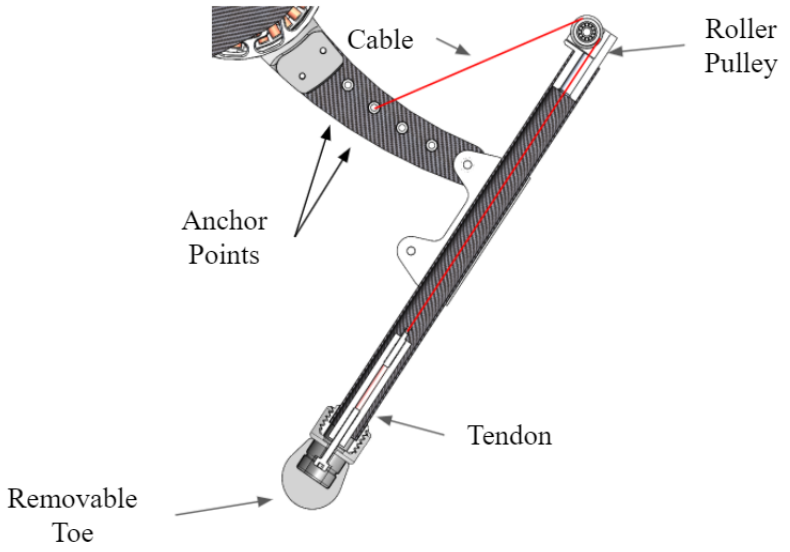

Figure 5: Cross-sectional view of the tendon mechanism.

3.2 Control

The robot uses a mode-switching PI controller (Figure 9) for continuous jumping. At each time step, a contact sensor provides ground-truth contact information, while magnetic encoders give absolute motor positions. The estimator (discussed below) uses these values to calculate positions and velocities both in joint space and the world frame, which in our case is the X-Z plane. We implemented two controllers in simulation and on hardware.

The simpler of the two controllers is the velocity sign-switch controller. It takes contact status, vertical velocity, and vertical position as inputs, with position and velocity measured at the center of the hip motor. While airborne (the contact sensor reads false), the controller commands joint positions through Odrive's internal position controller. When the foot is in contact with the ground, the controller sends torque commands. If the vertical velocity is negative, the controller commands zero torque. Otherwise, it commands joint torques calculated using the Jacobian from the head to the toe and a desired ground reaction force (i.e. $\tau = J^T F$). During each flight phase, the maximum height is recorded and compared to the desired jump height to calculate an error. Using proportional and integral gains, the desired ground reaction force is adjusted accordingly.

The other controller we have implemented wraps joint position thresholds around the velocity sign-switch scheme described above. This eliminates the need for an assumption that the robot will "bottom out" and switch direction on its own, either by fully extending the tendon or, as happened in practice, slamming against the mechanical hard stops and slightly bouncing upwards.

On our hardware, it turns out that the simpler sign-switching scheme worked well enough consistently, so we used this controller during data collection.

3.3 Estimation

Any type of closed loop controller requires precise state information to compute the control signal to send to the motors. Since we deployed our software on a Raspberry Pi for the hardware experiments, we were able to reuse the same code that we tested, tuned and verified in the simulator by simply remapping the inputs from simulated sensors to real sensors. The state estimator has two different modes of operation, one for the contact phase and one for the aerial phase. When in contact, we treat our robot as a parallel manipulator anchored at the ground and use forward kinematics to compute the toe displacement, body position and body velocity. When in the flight phase, we apply gravitational and frictional terms to update the body vertical velocity of the robot and integrate again to get the body vertical position. This type of estimator is inspired by the approach presented in [14]. This form of double integration tends to drift significantly over longer periods of time [15], but since we're able to directly measure all aspects of the state each time we hit the ground we assumed that this drift will not be significant in the < 1s aerial phase. This assumption can be validated by our simulation test results where we demonstrate that we can track the current state of the robot through different contact modes effectively (see Figure 10 in the Appendix).

4 Methods

Our original plan was to run a full-factorial study on power consumption while successively jumping to specified heights with different spring configurations. Upon further consideration, we decided that a fractional-factorial design was more appropriate given that considering other variables—such as spring pretension and stiffness for each configuration, or alternative controller options—would not have fit within the scope of this course due to the time and resources required.

It is important to note here that we define a spring configuration by the mounting point of the wire connected to the tendon, and we used the same tendon for all of our experimentation. Different configurations have the same stiffness but different pretensions and initial lengths. Due to the geometry of the mounting locations, different configurations also have different relationships between extensor motor angle and tendon force, with the mounting point closest to the tendon having the smallest effective angle range.

Ultimately, we decided to record electrical input to the motors, contact status, and average jump height while varying 2 parameters: spring configuration and target height. Each trial was to consist of 10 consecutive jumps, and we would run 5 trials at each spring configuration/target height pair. With 4 possible spring configurations and 2 possible target heights, this would have yielded a total of 40 trials. For each run, we would discard the trials showing the highest and lowest average heights, using the remainder for analysis.

In practice, the robot jumped more consistently than we had anticipated, so we logged 3 trials (instead of 5) at each configuration and did not discard any data. Due to time constraints and the occasional need to debug hardware issues, we ran trials for 1 target height instead of 2. Given that we are primarily interested in how the tendon configuration affects efficiency, we prioritized testing all 4 configurations over multiple commanded heights.

5 Results

Our collected data is summarized in Table 1 and a visualization of the efficiency (measured in units of meters of jump height per watt of input power) is shown in Figure 6.

Table 1	Average Height (m)	Average Power (watts)
Configuration 1	0.61	22.7
Configuration 2	0.64	22.0
Configuration 3	0.66	20.1
Configuration 4	0.69	18.1

Table 1: Spring Configuration Jump Results

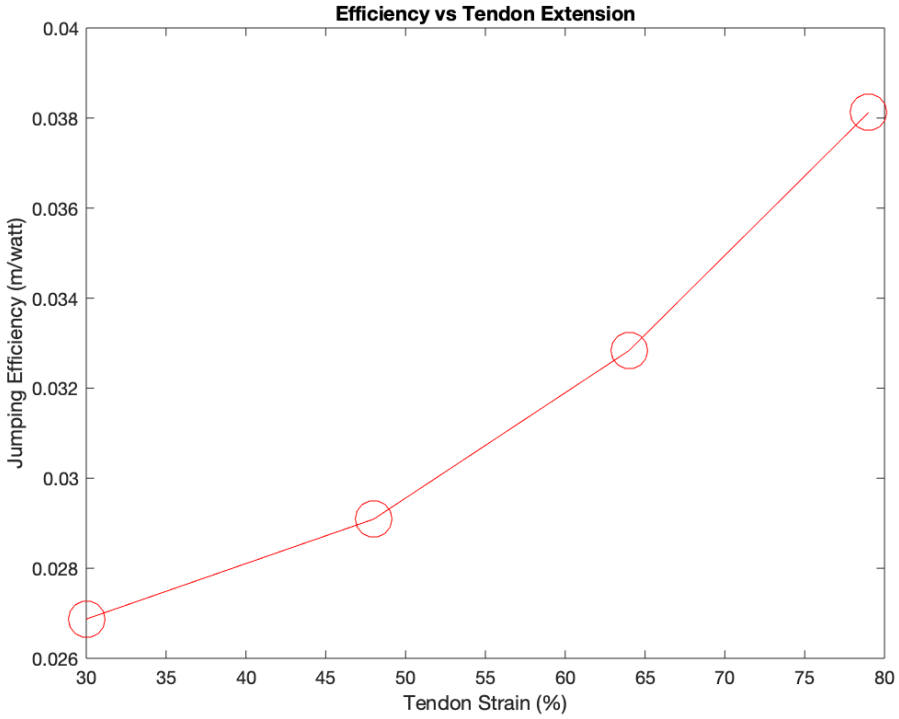

Figure 6: Efficiency of each Spring Configuration

We see a clear positive correlation between the tendon strain percentage and our overall jumping efficiency. This backs up our hypothesis that longer tendons that are designed to extend more are more energy-efficient in persistent jumping tasks. To show both the repeatability of our test setup as well as the gap between different tendon extensions, we now isolate our longest and shortest tendon attachment points and draw 2σ covariance ellipsoids [16] around each configuration.

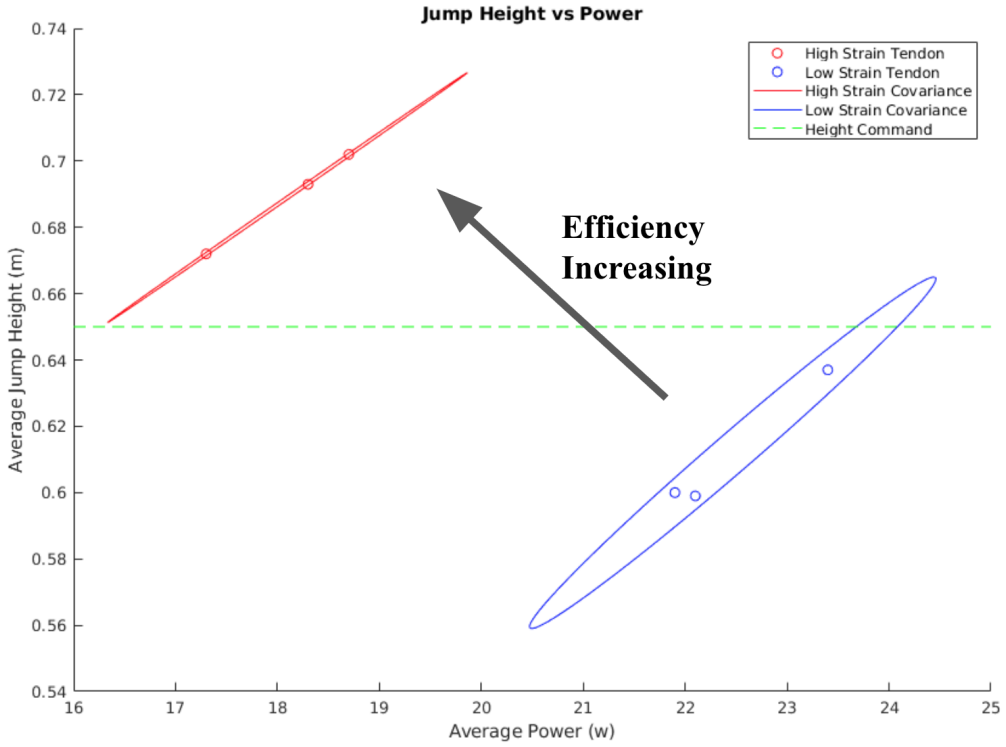

Figure 7: Efficiency of Longest and Shortest Tendon Configurations

6 Conclusions and Future Work

In this report, we address the issue of energy efficiency in legged robots and draw inspiration from kangaroos in the design of a monopod hopper. Our initial experiments confirm our hypothesis that as tendon strain increases, the energetic cost of successive hopping to a constant height decreases. In the future, we hope to conduct a more extensive study, searching for an optimal tendon strain function with respect to energy efficiency. We would also like to explore the full design space of spring configurations possible with this robot, exploring stiffness, strain percentage, and pretension as they pertain to energy efficiency. With some mechanical modifications, our platform could also be used to assess the merits of parallel vs. series spring configurations. With a full planar test rig such as a boom, and a more advanced control architecture, our robot could be used to explore planar hopping and running.

Small scale test-beds like the one built in this work can be used to quickly and cheaply assess leg designs before scaling them up to expensive human-scale, high degree-of-freedom systems. While there are many trade-offs when introducing compliance to legged systems not discussed in this report, such as actuator bandwidth and negative work due to motors fighting parallel springs, we believe that our conclusions make a strong case for the use of elastic energy storage elements in legged robot design.

References

[1] "Boston dynamics spot press release," 2020.

[2] J. K. Yim and R. S. Fearing, "Precision jumping limits from flight-phase control in salto-1p," in *2018 IEEE/RSJ International Conference on Intelligent Robots and Systems (IROS)*, pp. 2229–2236, IEEE, 2018.

[3] D. W. Haldane, J. K. Yim, and R. S. Fearing, "Repetitive extreme-acceleration (14-g) spatial jumping with salto-1p," in *2017 IEEE/RSJ International Conference on Intelligent Robots and Systems (IROS)*, pp. 3345–3351, IEEE, 2017.

[4] R. M. Alexander and A. Vernon, "The mechanics of hopping by kangaroos (macropodidae)," *Journal of Zoology*, vol. 177, no. 2, pp. 265–303, 1975.

[5] R. Kram and T. J. Dawson, "Energetics and biomechanics of locomotion by red kangaroos (macropus rufus)," *Comparative Biochemistry and Physiology Part B: Biochemistry and Molecular Biology*, vol. 120, no. 1, pp. 41–49, 1998.

[6] B. Brown and G. Zeglin, "The bow leg hopping robot," in *Proceedings. 1998 IEEE International Conference on Robotics and Automation (Cat. No.98CH36146)*, vol. 1, pp. 781–786 vol.1, 1998.

[7] V. Klemm, A. Morra, C. Salzmann, F. Tschopp, K. Bodie, L. Gulich, N. Küng, D. Mannhart, C. Pfister, M. Vierneisel, F. Weber, R. Deuber, and R. Siegwart, "Ascento: A two-wheeled jumping robot," in *2019 International Conference on Robotics and Automation (ICRA)*, pp. 7515–7521, 2019.

[8] C. Zhang, W. Zou, L. Ma, and Z. Wang, "Biologically inspired jumping robots: A comprehensive review," *Robotics and Autonomous Systems*, vol. 124, p. 103362, 2020.

[9] "Western australia police investigate 'sickening' kangaroo killings," 2018.

[10] A. Abate, *Mechanical Design for Robot Locomotion*. PhD thesis, Oregon State University, 2018.

[11] A. Abate, J. W. Hurst, and R. L. Hatton, "Mechanical antagonism in legged robots.," in *Robotics: Science and Systems*, vol. 6, Ann Arbor, MI, 2016.

[12] M. M. Plecnik, D. W. Haldane, J. K. Yim, and R. S. Fearing, "Design Exploration and Kinematic Tuning of a Power Modulating Jumping Monopod," *Journal of Mechanisms and Robotics*, vol. 9, 12 2016. 011009.

[13] T. M. Inc., *Simscape Multibody*. Natick, Massachusetts, United States, 2020.

[14] M. Bloesch, M. Hutter, M. A. Hoepflinger, S. Leutenegger, C. Gehring, C. D. Remy, and R. Siegwart, "State estimation for legged robots-consistent fusion of leg kinematics and imu," *Robotics*, vol. 17, pp. 17–24, 2013.

[15] H. Yan, Q. Shan, and Y. Furukawa, "Ridi: Robust imu double integration," in *Proceedings of the European Conference on Computer Vision (ECCV)*, September 2018.

[16] M. Friendly, G. Monette, J. Fox, *et al.*, "Elliptical insights: understanding statistical methods through elliptical geometry," *Statistical Science*, vol. 28, no. 1, pp. 1–39, 2013.

7 Appendix I: Individual Technical Contributions

7.1 Technical Contribution: Benjamin Bokser

Benjamin Bokser led the overall mechanical design of the robot. He was responsible for design conceptualization, component selection, and CAD.

7.2 Technical Contribution: Nicholas Jones

Nicholas was responsible for writing the controllers and testing them in simulation and on hardware.

7.3 Technical Contribution: Nikolai Flowers

Nikolai designed and implemented the mode-switching state estimator, the electronics harness and all of the high-level motor control interfacing functions.

7.4 Technical Contribution: Joseph Wood

Joseph designed much of the lower leg, including the carbon fiber tube and adjustable spring mechanism. He evaluated various spring materials and performed analysis to select a spring appropriate for hopping given task requirements. He built the reduced-order model in simulink for verifying motor selection, link lengths, and spring stiffness before implementation in mechanical design. Finally, he led mechanical fabrication of the robot, making machined and waterjet parts in the CMU machine shop.

8 Appendix II: Budget

PART NAME	DESCRIPTION	QTY.	SALES VOLUME	PURCHASE QTY.	ALREADY OWNED?	PRICE	TOTAL	VENDOR	LINK
47065T513	3x1 T-Slotted Structure	1	1	1	$1.00	$39.06	$39.06	McMasterCarr	https://www.mcma
9246K13	12x12x.25 Flat Bar Alum	1	1	1	$1.00	$33.12	$33.12	McMasterCarr	https://www.mcma
MGN12 1000mm	Linear Rail + Carriage	1	1	1	$1.00	$53.99	$53.99	Amazon	https://www.amazo
47065T139	End-Feed Single Nut with	4	1	4	$1.00	$1.85	$7.40	McMasterCarr	https://www.mcma
200x300x4.0MM 1	Carbon Fiber Plate	1	1	1	$1.00	$50.90	$50.90	Amazon	https://www.amazo
8974K11	3/4" Diameter x 1foot Alu	1	1	1	$1.00	$4.15	$4.15	McMasterCarr	https://www.mcma
8974K15	1-1/8" Diameter 6061 Alu	1	1	1	$1.00	$5.49	$5.49	McMasterCarr	https://www.mcma
8974K71	2" Diameter 6061 Alumin	1	1	1	$1.00	$15.21	$15.21	McMasterCarr	https://www.mcma
4668K113	Stainless Steel Ball Bear	6	10	1	$1.00	$47.37	$47.37	VXB	https://www.vxb.co
SMR104-ZZ	Stainless Steel Ball Bear	1	1	1	$1.00	$3.95	$3.95	VXB	https://www.vxb.co
MGN12C	Reliabot MGN12C Carria	2	1	2	$1.00	$14.99	$29.98	Amazon	https://www.amazo
94669A005	Aluminum Unthreaded S	5	1	5	$1.00	$1.66	$8.30	McMasterCarr	https://www.mcma
57155K496	Flanged Ball Bearing, St	4	1	4	$1.00	$7.84	$31.36	McMasterCarr	https://www.mcma
4PCS 16mm	Carbon Fiber Tube 14x1	1	4	1	$1.00	$14.99	$14.99	Amazon	https://www.amazo
Copper Foil Tape (1 inch X 33 FT)	Copper Tape	1	1	1	$1.00	$8.98	$8.98	Amazon	https://www.amazo
91294A128	Black-Oxide Alloy Steel F 90 Degree Countersink A	8	100	1	$1.00	$5.04	$5.04	McMasterCarr	https://www.mcma
93497A120	Steel Spring Lock Washe Conical, DIN 6796, for M	2	100	1	$1.00	$7.24	$7.24	McMasterCarr	https://www.mcma
91100A120	Zinc-Plated Steel Oversi for M3 Screw Size, 3.2 m	2	100	1	$1.00	$2.66	$2.66	McMasterCarr	https://www.mcma
97763A813	18-8 Stainless Steel Butt Black Oxide, M3 x 0.50 r	2	10	1	$1.00	$7.00	$7.00	McMasterCarr	https://www.mcma
92125A104	18-8 Stainless Steel Hex M4 x 0.7 Thread Size, 15	3	100	1	$1.00	$7.20	$7.20	McMasterCarr	https://www.mcma
92125A103	18-8 Stainless Steel Hex M3 x 0.5 Thread Size, 15	4	100	1	$1.00	$4.72	$4.72	McMasterCarr	https://www.mcma
91294A133	Black-Oxide Alloy Steel F 90 Degree Countersink,	10	100	1	$1.00	$7.16	$7.16	McMasterCarr	https://www.mcma
94180A331	Tapered Heat-Set Inserts Brass, M3 x 0.50 mm Thr	9	100	1	$1.00	$13.35	$13.35	McMasterCarr	https://www.mcma
98055A087	1074-1095 Spring Steel F 0.3mm Thick, 4mm ID	3	50	1	$1.00	$3.00	$3.00	McMasterCarr	https://www.mcma
90323A217	18-8 Stainless Steel Low 4 mm Shoulder Diameter	1	1	1	$1.00	$3.82	$3.82	McMasterCarr	https://www.mcma
93501A009	Steel Belleville Spring Lo for Number 8 and M4 Sc	3	100	1	$1.00	$7.71	$7.71	McMasterCarr	https://www.mcma
99178A101	Heavy Duty Side-Mount F Black Phosphate 1060-1	1	100	1	$1.00	$8.70	$8.70	McMasterCarr	https://www.mcma
90323A439	18-8 Stainless Steel Low 4 mm Shoulder Diameter	2	1	2	$1.00	$5.50	$11.00	McMasterCarr	https://www.mcma
5234K66	Super-Soft Latex Rubber	1	1	1	$1.00	$8.30	$8.30	McMasterCarr	https://www.mcma
91290A172	Black-Oxide Alloy Steel S M4 x 0.7 mm Thread, 30	1	5	1	$1.00	$3.71	$3.71	McMasterCarr	https://www.mcma
95907A170	Corrosion-Resistant Exte M4 x 0.7 mm Thread Size	1	1	1	$1.00	$8.57	$8.57	McMasterCarr	https://www.mcma
3450T37	Galvanized Steel Wire R	1	1	1	$1.00	$11.75	$11.75	McMasterCarr	https://www.mcma
694ZZ	Donepart 694ZZ Bearing	1	1	1	$1.00	$10.98	$10.98	Amazon	https://www.amazo
ODrive Motor Con	2-axis FOC Controller	1	1	1	$0.50	$135	67.5	ODrive	https://odriverobot
8318 Motor	8318 Direct Drive BLDC	1	1	1	$0.50	65	$32.50	Aliexpress	https://www.aliexp
T-Motor	T-Motor	1	1	1	0.5	98.22	49.11	T-Motor	https://www.getfpv
AS5047 Encoder	AS5047 Mag Encoder	1	1	2	1	15.75	31.5	Mouser	https://www.mouse

Figure 8: Final Budget. Total expenses came out to $717.66

The spreadsheet of expenses can be found here.

9 Appendix III: Additional Figures

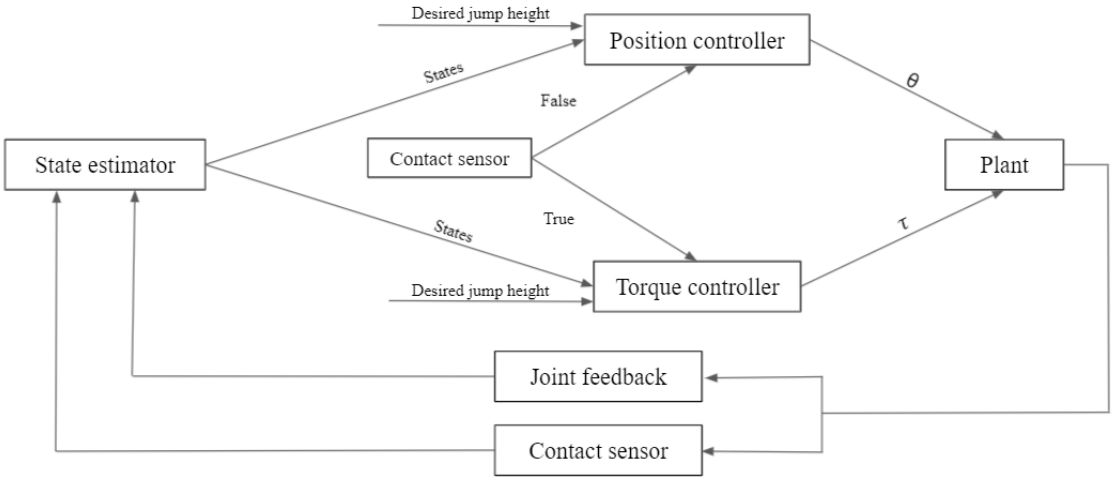

Figure 9: Block diagram of the mode switching controller.

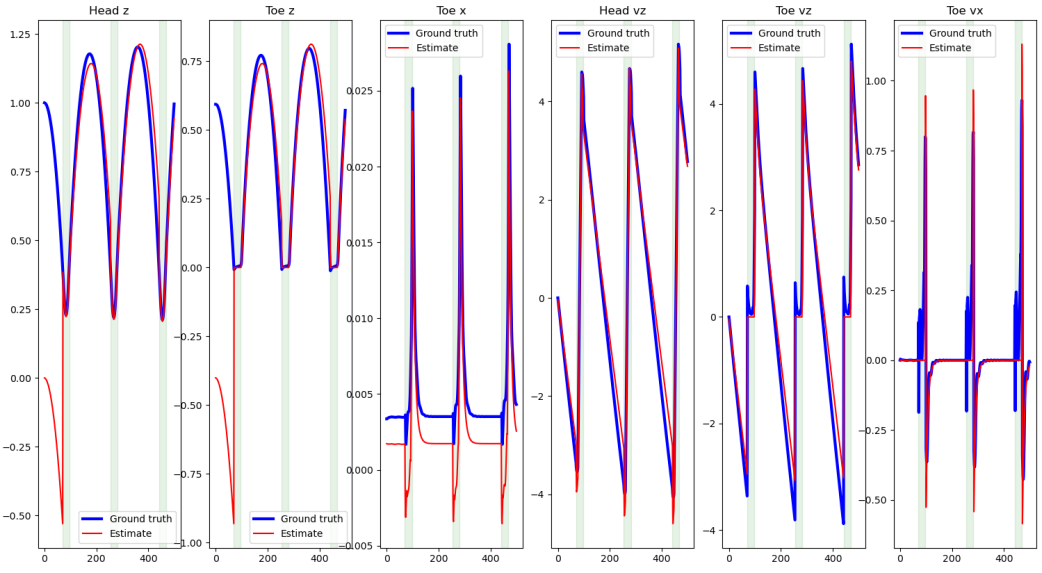

Figure 10: Switching State Estimator Accuracy

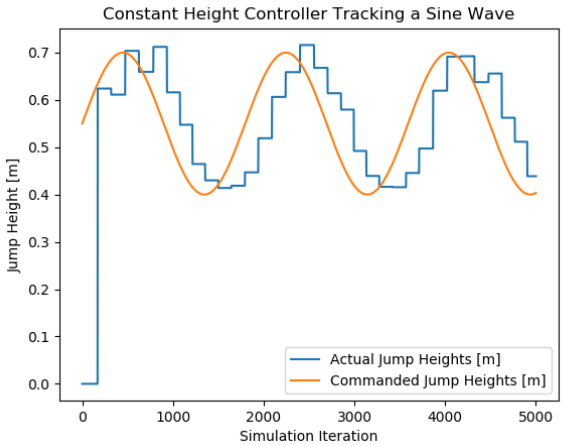

Figure 11: Simulated robot tracking a sine wave of desired jump height inputs

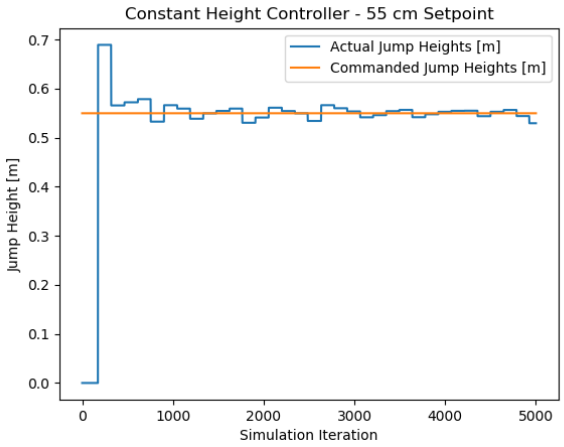

Figure 12: Simulated robot achieving a constant jump height of 55 cm

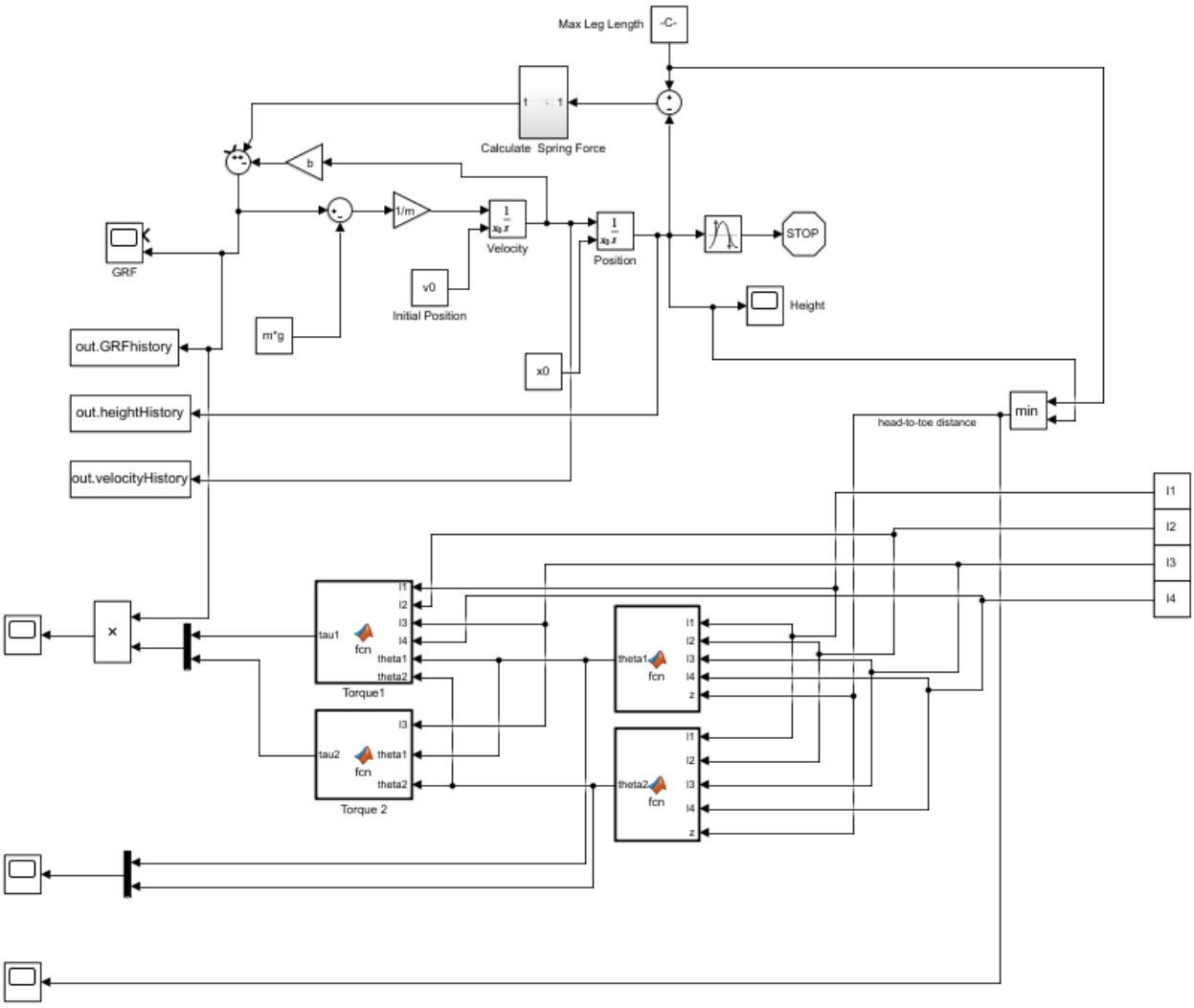

Figure 13: First-Order Simulink Model used to obtain torque requirements

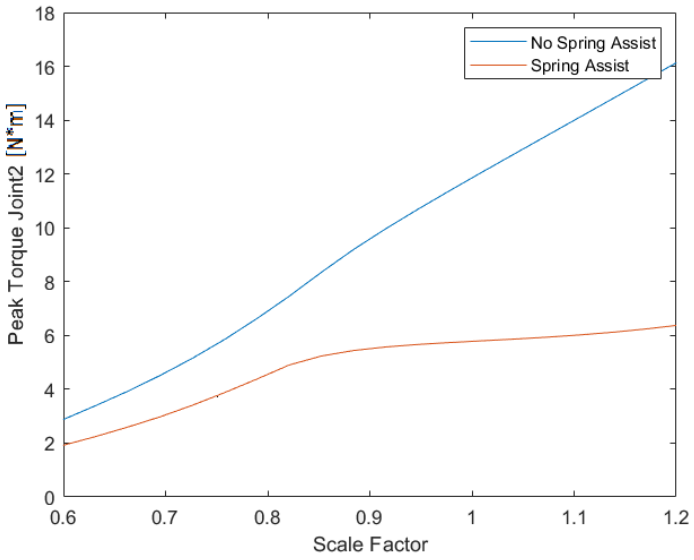

Figure 14: Scaling analysis of peak torque requirement in the extensor motor as link lengths scale evenly. We used this plot to decide to scale down our link lengths to 75 percent of their original lengths in order to keep peak joint torques below a safe level.

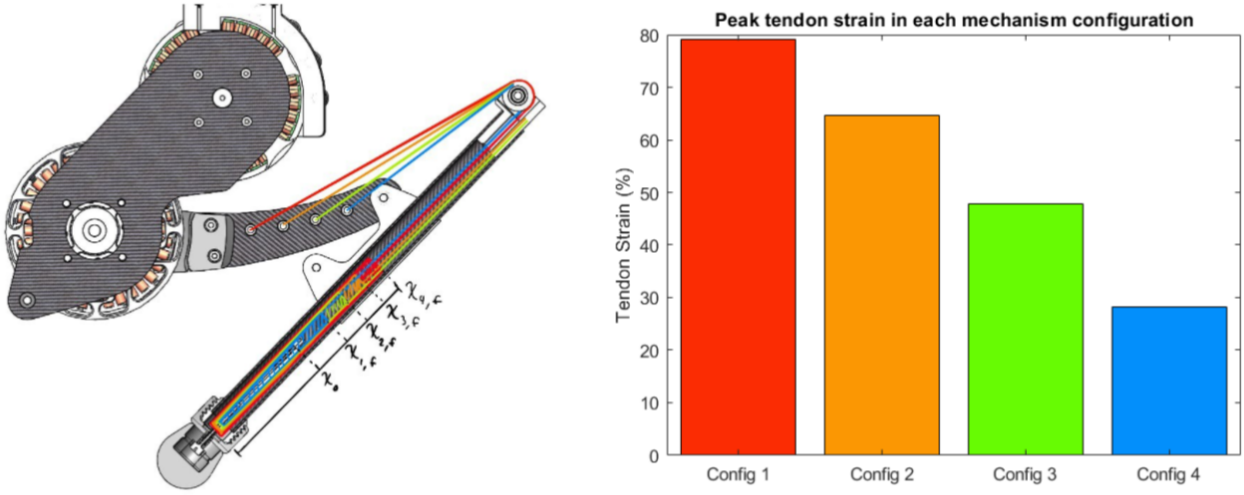

Figure 15: Comparison of strain percentage for each configuration.